J. Fluid Mech. (2005), *vol.* 533, *pp.* 223–236.
doi:10.1017/S0022112005003952 Printed in the United Kingdom

Mixing and segregation of granular matter: multi-lobe formation in time-periodic flows

By S. J. FIEDOR AND J. M. OTTINO

Department of Chemical Engineering, Northwestern University, Evanston, IL 60208, USA

(Received 30 August 2004 and in revised form 22 January 2005)

We study size segregation in two classes of granular systems in time-periodically forced quasi-two-dimensional tumblers. In dry granular systems (DGS), particles are immersed in air, whereas in liquid granular systems (LGS) or slurries, particles are wholly immersed in a less dense liquid. Experimental results show lobe formation and classical radial segregation, depending on the frequency of the forcing and fill fraction of the system. Both DGS and LGS exhibit similar multi-lobe patterns when subjected to the same forcing. A simple model captures the experimental results and suggests that the symmetry of the forcing plays a crucial role in the emergence of the patterns. Lobes form via a reinforcement mechanism that depends on the period of the regular islands in the Poincaré map. The mechanism can be controlled by changing the forcing period and/or fill fraction.

1. Introduction

Flowing granular matter is ubiquitous – examples abound in nature and technological applications. Ubiquity, however, has not resulted in a comparable level of understanding and over the last few years there has been a substantial amount of work trying to elucidate the often-baffling behaviour of flowing granular matter. Furthermore, the interstitial fluid can complicate matters. In this study, two kinds of granular systems are considered – dry granular systems and liquid granular systems. In dry granular systems (DGS), particles are immersed in air, whereas in liquid granular systems (LGS) or slurries, particles are wholly immersed in a less dense liquid. It is important to stress that DGS and LGS are two-phase systems, either particles and air or particles and a liquid. With only a few exceptions, nearly all of the voluminous research on granular flows during the last decade has focused on DGS. Only a handful of studies have addressed the motion of materials in LGS, and notable among them have been several recent studies focusing on patterns in rotating cylinders in the related field of suspensions (Tirumkudulu, Tripathi & Acrivos 1999; Thomas *et al.* 2001; Duong, Hosoi & Shinbrot 2004; Jin & Acrivos 2004). The physics of these systems is undoubtedly different from the systems considered here. The noteworthy result is that monodisperse neutrally buoyant particles partially filling a horizontal rotating cylinder, under certain conditions, segregate into bands of particles separated by regions of low particle concentrations.

One system that has become prototypical in mixing and pattern-formation studies is the quasi-two-dimensional circular tumbler. Rotated cylindrical tumblers filled with binary mixtures of large/small (S-systems) or dense/less-dense materials (D-systems) separate radially in the plane perpendicular to the axis of rotation, forming a classical radial segregation pattern in the case of a circle and, typically, two rotating lobes

in the cases of squares filled exactly half-full (Hill *et al.* 1999). This process occurs quickly, within a single rotation, and has been observed in both DGS and LGS. A continuum model of flow and segregation in a circular tumbler was proposed by Khakhar *et al.* (1997) and applied by Hill *et al.* (1999) to mixing and segregation of DGS in two-dimensional containers – elliptic and square – where the flow, interpreted in a continuum sense, is chaotic. More recently, the model was extended to flow in three-dimensional systems (Gilchrist & Ottino 2003). In all the cases studied to date, the container rotates at a steady rotation rate, the single exception being the work of Hill, Gioia & Amaravadi (2004).

It is, however, clear that mixing often takes place in systems where the *flow within the container* is time-periodic–the time-periodicity arising owing to the steady rotation of a non-spherical shape such as a square or a cube. Mixing in three-dimensional geometries presents problems of its own and very few works have addressed this subject; the two-dimensional case is undoubtedly simpler. However, there is an even simpler case that has yet to be studied in detail: a circular container rotated in a time-dependent manner. It is prudent to start with such a case.

There are two inter-related objectives of the present paper. The first is to uncover similarities – to present a side-by-side comparison of mixing and segregation of DGS and LGS; to what extent do both systems produce similar results when subject to the same forcing? The second objective is to find out how well the results can be interpreted in terms of a single model that depends solely on the underlying flow. In order to produce the strictest testing and comparison, the systems will be operated in such a way that the underlying motion, interpreted in a continuum sense, is chaotic. This produces segregated structures that are strikingly different from regular flow and therefore serves as a way to highlight possible variations between model predictions and experimental results.

2. Forcing of system

The system is periodically forced with an angular velocity

$$\omega = \omega_{ave} + \omega_{amp} \sin(2\pi f_E t), \tag{2.1}$$

where ω_{ave} is the average angular velocity, ω_{amp} is the amplitude of oscillation, and f_E is the forcing frequency of the experiment. The rotation is restricted to only one direction. That is, ω_{ave} is greater than zero and ω_{amp} is less than ω_{ave},

$$0 < \omega_{amp} < \omega_{ave}. \tag{2.2}$$

This ensures that the maximum angular velocity (ω_{max}) and minimum angular velocity (ω_{min}) are both positive. The forcing frequencies are such that there is an integer number of cycles per revolution, i.e.

$$f_E = \underbrace{\text{integer}}_{(\text{cycles rev}^{-1})} \; \underbrace{\omega_{ave}}_{(\text{rev s}^{-1})}. \tag{2.3}$$

This constrains the system to be rotationally symmetric every 1/integer revolutions (see figure 1). Note that the system has a time-dependent angular velocity, $\omega(t)$, and angular acceleration, $\mathrm{d}\omega(t)/\mathrm{d}t$, but owing to the rotational symmetry ω and $\mathrm{d}\omega/\mathrm{d}t$ can be viewed as position dependent. Figure 1(*a*) shows the dependence of ω viewed with respect to time (bottom axis, solid line) and angular position (θ) (top axis, dashed line) corresponding to a system with a forcing frequency of 4 cycles rev^{-1}. Figure 1(*b*) shows ω on polar coordinates of θ for the same system. This plot serves

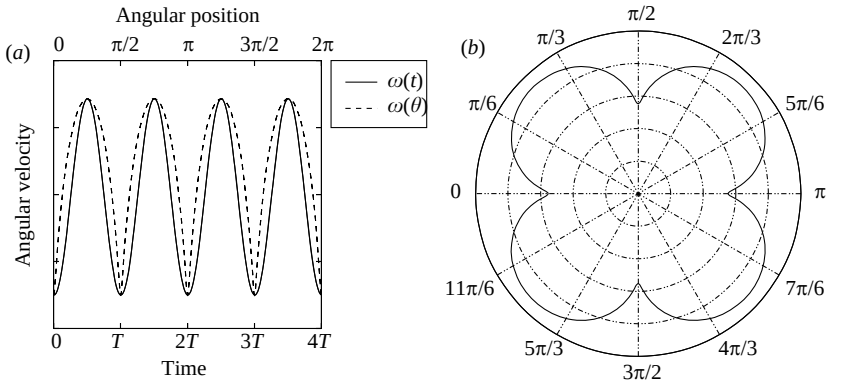

FIGURE 1. Symmetry of the time-forcing protocol. (*a*) Angular velocity plotted as a function of time and angular position corresponding to a system with a forcing frequency of 4 cycles rev^{-1}; it takes a time $4T$ to complete one revolution. (*b*) Angular velocity as a function of angular position plotted on polar coordinates. A point starting at $\theta = 0$ starts at the minimum speed and then undergoes four cycles of acceleration and deceleration.

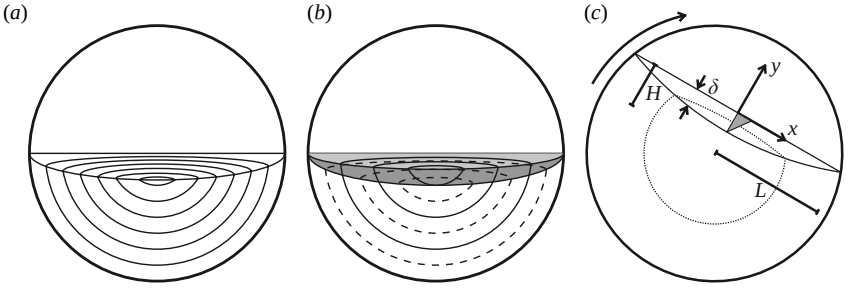

FIGURE 2. (*a*) Particle streamlines in a circular tumbler rotated at a steady rotation rate. (*b*) Particle streamlines in a circular tumbler at two different rotation rates. Note the crossing streamlines in the flowing layer. (*c*) Schematic of the model.

to highlight the rotational symmetry of the system. When the tumbler is at position $\theta = 0$, the angular velocity is at a minumum. As the tumbler rotates, it accelerates until it reaches the maximum angular velocity at $\theta = \pi/4$, and then decelerates to the minimum angular velocity at $\theta = \pi/2$, and so on. In general, symmetries may arise owing to the geometry of the container as well as the forcing protocol. In this paper, the system is restricted to circular containers, and therefore the symmetry is solely dependent on the forcing.

3. Details of the model

The continuum model used here (based on the work of Khakhar *et al.* 1997, 1999) is simple. The model describes the mean flow; thus the material in the tumbler is assumed to be homogeneous, rather than consisting of different kinds of particles. Further, we assume that the flow consists of two distinct regions: a flowing layer with nearly unidirectional flow and a bed below it undergoing solid-body rotation, see figure 2. This is an approximation; experiments show the velocity in the flowing layer decreases exponentially with depth, rather than being a sharp transition between the

two regions (Komatsu *et al.* 2001; Jain, Ottino & Lueptow 2002). However, this is an excellent approximation for short time scales.

The shape of the flowing layer–bed interface is taken as

$$\delta = \delta_0 \left(1 - \frac{x^2}{L^2}\right)^{1/2}, \tag{3.1}$$

where δ_0 is the maximum layer thickness (at $x = 0$) and L is the layer length (Makse 1999; Khakhar, Orpe & Ottino 2001). Note that the dynamic angle of repose and the thickness of the flowing layer depend on the thickness of the container and the friction at the walls (Taberlet *et al.* 2003). Experiments also show that the thickness of the flowing layer depends on ω (Khakhar *et al.* 1997). In the model, this is accounted for by changing δ_0. The free surface of the system is assumed to be flat and does not move. To incorporate the changing thickness of the flowing layer with ω, δ_0 is made time dependent,

$$\delta_0 = \delta_{0,ave} + \delta_{0,amp} \sin(2\pi f_E t), \tag{3.2}$$

where $\delta_{0,ave}$ is the average maximum layer thickness and $\delta_{0,amp}$ is the amplitude of oscillation. The oscillating flowing-layer thickness results in streamline crossing; i.e. streamlines show transversal intersections when streamline portraits corresponding to different rotation rates are superposed (see figure 2). This results in a chaotic flow (Ottino (1989)).

Particles in the bed move with the same velocity as the tumbler,

$$v_r = 0 \tag{3.3}$$

and

$$v_\theta / r = \omega_{ave} + \omega_{amp} \sin(2\pi f_E t). \tag{3.4}$$

Material is continuously avalanching downward in the flowing layer. Both collisional diffusion and segregation of particles are neglected. A linear velocity profile is assumed in the streamwise direction,

$$v_x = \frac{\omega L^2}{\delta_0} \left(1 - \frac{y}{\delta(x)}\right), \tag{3.5}$$

where x and y are coordinate positions as defined in figure 2. Using $\delta(x)$ from (3.1), v_x from (3.5) and the continuity equation, the velocity profile in the transverse direction is determined to be

$$v_y = \frac{-\omega \delta_0 x y^2}{2\delta^3(x)}. \tag{3.6}$$

The values of $\delta_{0,ave}$ and $\delta_{0,amp}$ are approximated from experimental observation and result in δ_0 ranging from $0.05L$ to $0.1L$ in the half-full system. There is theoretical guidance relating the thickness of the flowing layer and its dependence with ω (Khakhar *et al.* 2001). Numerical simulations show that the results are insensitive to the values of δ_0.

4. Maps

The velocity field of the granular material within the container, $\boldsymbol{v}(\boldsymbol{x}, t)$, interpreted from a continuum viewpoint, is time-periodic, i.e. $\boldsymbol{v}(\boldsymbol{x}, t) = \boldsymbol{v}(\boldsymbol{x}, t + T)$. Such systems can be reduced to a mapping $\phi(\boldsymbol{x})$. In a period T, $\boldsymbol{x}_n$ is mapped to $\boldsymbol{x}_{n+1}$, $\boldsymbol{x}_{n+1} = \phi(\boldsymbol{x}_n)$;

i.e. if initial conditions are denoted as $\boldsymbol{x}_0$, $\boldsymbol{x}_n = \phi^n(\boldsymbol{x}_0)$. Periodic points are such that $\boldsymbol{p} = \phi^n(\boldsymbol{p})$, where n is the period of the point. Thus a periodic point of order 1 returns back to position $\boldsymbol{p}$ after time $t = T, 2T, 3T, \ldots$; a periodic point of order 2 returns back to $\boldsymbol{p}$ after $t = 2T, 4T, 6T, \ldots$. Periodic points in two-dimensional systems can be classified as either elliptical or hyperbolic. The linearized flow near an elliptic point is a rotation or a twist; the linearized flow near a hyperbolic point is a contraction in one direction and a stretching in another. Elliptic points are surrounded by KAM curves; domains within KAM curves are called islands. Islands are invariant regions – material within an island remains within the island. In general, the largest visible islands are those with the lowest periods and within KAM curves there are additional higher-order periodic points, both hyperbolic and elliptic. The period of an island corresponds to the lowest-order periodic point and the boundary of an island to the outermost KAM curve.

A useful way of identifying the location of low-period islands and chaotic regions is by means of Poincaré sections. To compare the numerical results to experiments, Poincaré sections are made using the model in the following manner. Particles are initially placed at various locations in the bed. Particle positions are then determined by integrating the equations of motion in time. If a particle lies in the bed, (3.3) and (3.4) are used, whereas (3.5) and (3.6) are used for particles in the flowing layer. The positions of the particles are recorded after each period T (defined as $1/f_E$ or one cycle of acceleration and deceleration). Poincaré sections are then constructed by simply plotting all the recorded positions. Simulations are run for as many cycles as is necessary to resolve features such as small islands (usually less than 100 revolutions).

5. Experimental methods

The experimental set-up consists of a rotated tumbler that is partially filled with two different sized glass beads. The tumbler is made of acrylic and has a diameter of 178 mm and is 6.35 mm thick. It is rotated about its axis with a Compumotor LE57-51 stepper motor with a planetary gear drive. The angular velocity and angular acceleration are pre-programmed using Visual C++ before being sent to the motor. In the DGS experiments, the surrounding fluid is air, in the LGS experiments, the particles are completely immersed in water. An air pocket is present in some LGS experiments; however, this does not affect the results and the material never comes into contact with the air. The range of f_E studied is 3 to 8 cycles rev^{-1}.

In DGS experiments, the tumbler is filled with a binary mixture of 1.2 mm blue glass beads and 0.8 mm white zirconium silicate beads. The volume ratio of small to large beads is 1:2. In LGS experiments, the tumbler is filled with 0.8 mm clear glass beads and 0.3 mm black glass beads. The volume ratio of small to large beads is 1:4. Experiments are allowed to run for a few rotations, enough for a stable segregation pattern to form. Images of the patterns are then captured using a Kodak DC4800 digital camera. Experiments are run with various fill fractions for each f_E to try to capture many different patterns.

Long-time experiments are conducted in slurries for half-full systems. The Compumotor stepper motor is synchronized with a Kodak Megapixel 1.4i digital camera using a Visual C++ program. Images are taken every half-revolution for 4500 revolutions, resulting in 9000 total images. All the images are then merged together to form one image showing the long-time segregation pattern for each f_E.

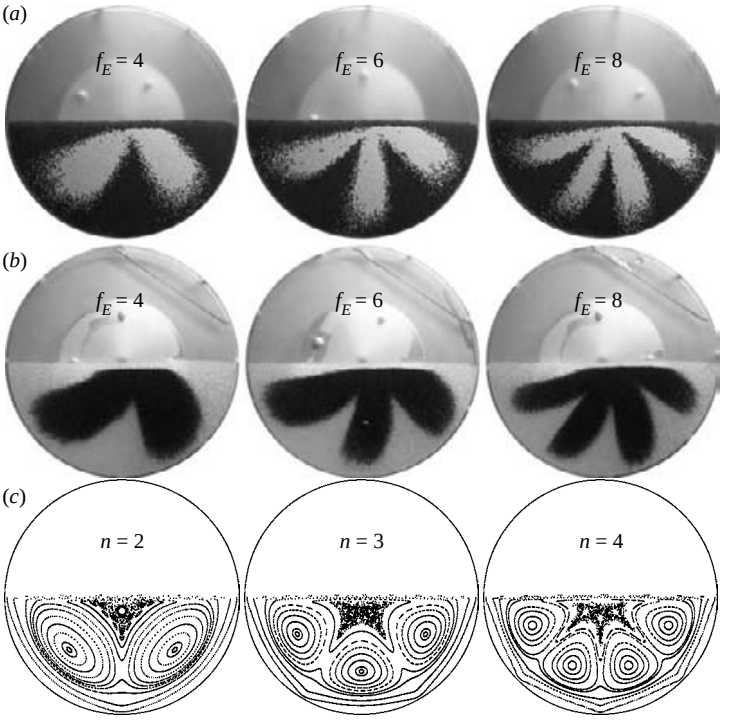

FIGURE 3. Results for a half-full tumbler with even f_E. (*a*) Experimental images from a DGS. (*b*) Experimental images from a LGS. (*c*) Poincaré sections from numerical simulation. The period of the elliptic points is denoted by n.

Particle-tracking experiments are also conducted in slurries for half-full systems with f_E of 3 and 6 cycles rev^{-1}. In these experiments, the tumbler is filled with a mixture of 1.0 mm and 1.7 mm clear glass beads with a small to large volume ratio of 3:2. One 1.0 mm bead is dyed black to distinguish it from all other particles. Images are taken every half revolution for 4500 revolutions, resulting in 9000 total images. The digital images are then read using Matlab, and the tracer particle's position is determined and recorded to a data file for quantitative analysis.

6. Results – half-full tumblers (DGS and LGS)

Results are presented in the following manner. First, we present experiments leading to lobe formation, followed by experiments where lobes do not form. These two results are used to develop a theory for the formation of lobes. The theory is then tested by seeking conditions that would result in further lobe formation.

Figures 3(*a*) and 3(*b*) are experimental images from half-full tumblers in DGS and LGS with even f_E (4, 6, and 8 cycles rev^{-1}). Smaller particles segregate from the larger particles forming lobes near the centre of the tumbler. These patterns form within a few revolutions and are stable. There is considerable agreement between DGS and LGS – each has the same number of lobes for the same f_E.

Figure 3(*c*) shows Poincaré sections corresponding to systems with similar f_E (4, 6 and 8 cycles rev^{-1}). The typical arrangement of regular regions – elliptic points surrounded by large regular islands – and chaotic regions are evident. The number of regular islands present in each case is $f_E/2$, similar to the number of lobes in the

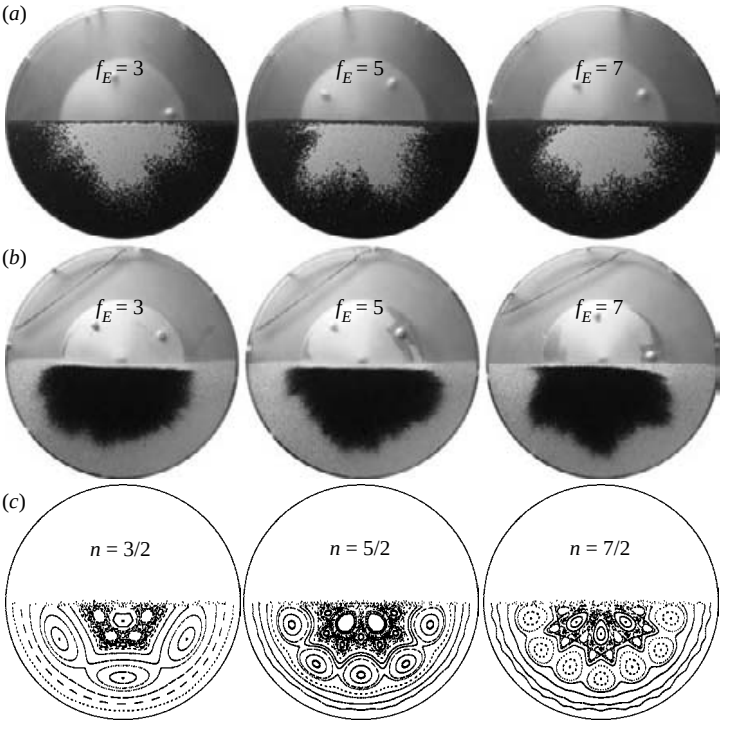

FIGURE 4. Results for a half-full tumbler with odd f_E. (*a*) Experimental images from a DGS. (*b*) Experimental images from a LGS. (*c*) Poincaré sections from numerical simulation. The period of the elliptic points is denoted by n.

experiments. The Poincaré section patterns are very sensitive to the fill fraction and a few per cent variation drastically changes the sizes of the regular islands.

Figure 4 shows experimental results for odd f_E (3, 5 and 7 cycles rev^{-1}). These results are strikingly different. Figures 4(*a*) and 4(*b*) are experimental images from a half-full tumbler in DGS and LGS. There is no clear lobe definition as in the case of systems with even f_E (figure 3). The companion Poincaré sections show there are regular and chaotic regions present (figure 4*c*), but the sizes of the regular islands are smaller than in the case of even f_E. There is also no apparent correspondence with the symmetries of the Poincaré sections. Smaller particles prefer to be near the core of the tumbler, forming a pattern similar to that of classical radial segregation seen in experiments carried out with steady rotation rates.

What accounts for this difference? Consider first the differences between the steady and time-periodic cases. Segregation occurs only in the flowing layer; particles in the bed are effectively locked until they re-enter the layer. In the steady rotation case, small particles fall downward, transverse with respect to the direction of the mean flow. The segregation mechanism (percolation) is always on; in just one or two rotations, the small particles self-organize, forming an invariant core (see figure 5). This is the standard radial segregation scenario. However, particles also segregate along the layer. Recent particle-tracking velocimetry (PTV) experiments performed in flowing granular layers in systems with particles of different sizes show that the smaller particles travel faster than the larger particles (Jain, Ottino & Lueptow 2004). To a first approximation, the speed of the flowing particles depends on the size, and

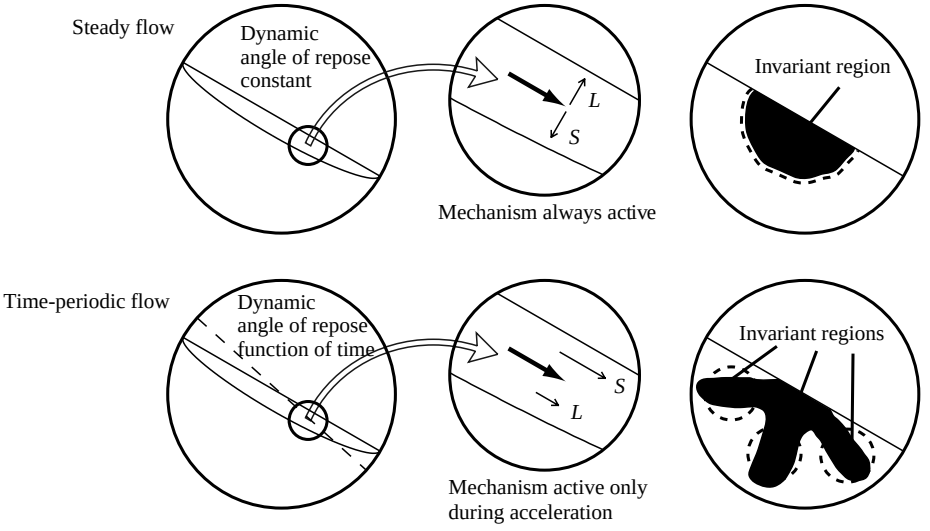

FIGURE 5. Top – Segregation in a system with a steady rotation rate. Smaller particles percolate down through the flowing layer toward the centre of the tumbler. Bottom – Segregation when system is accelerating. Smaller particles still percolate through the flowing layer, but they also travel farther down the flowing layer.

weakly on the density. Depending on the ratio of particle sizes, the difference in particle speed can be quite significant.

Careful visualization of the experiments suggests the following mechanism for lobe formation and the subsequent stability of the patterns. Segregation in the direction of the flow depends strongly on the forcing. During acceleration, smaller particles flow faster than larger ones and also farther down the flowing layer compared with a system operating at a steady rotation rate. When the system is decelerating, the effect is diminished. In half-full systems the periods of the elliptic points are $f_E/2$. Thus islands in systems with even f_E have periods with integer values, while islands in systems with odd f_E have periods with non-integer values. In half-full systems with even f_E, the period of the elliptic points are commensurate with the cycle time of the forcing. Therefore when the elliptic points return to their original positions, in particular as they re-enter the layer, they encounter exactly the same forcing (velocity, acceleration) as they did on the previous entrance. Resonance occurs, and any dynamical effect such as fingering is reinforced (see figure 5). Small particles exit the layer and fall in the location occupied by the islands; once there, since the islands are invariant regions, material is 'trapped' and the pattern is frozen. By contrast, the islands in systems with an odd f_E encounter a forcing that is out of phase by half a cycle from the previous time; acceleration in one period, deceleration in the next period. Dynamical effects are cancelled. Figure 4(a) shows lobes beginning to form for a system with $f_E = 7$. Since the tumbler is half-full, three and a half lobes begin to form, but the lobes do not fully emerge because there is no reinforcement mechanism.

7. Results – more than half-full tumblers (DGS and LGS)

The results in the previous section are restricted to half-full systems. We argue that lobes form when there exists a reinforcement mechanism due to islands having

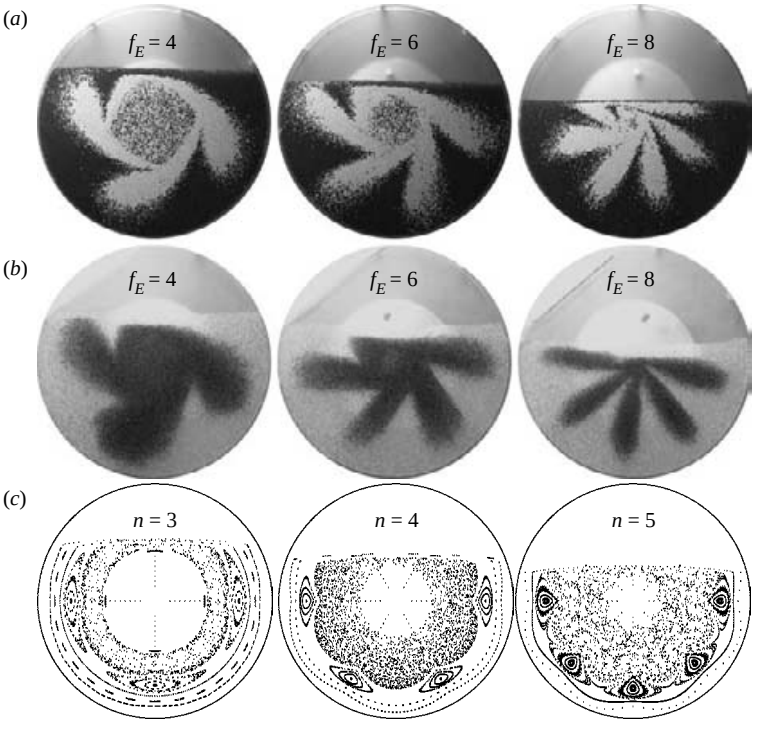

FIGURE 6. Results for a tumbler more than half-full with even f_E. (*a*) Experimental images from a DGS. The fill fractions are 0.79, 0.72 and 0.62 by area. (*b*) Experimental images from a LGS. The fill fractions are 0.77, 0.69 and 0.60 by area. (*c*) Poincaré sections from numerical simulation. The fill fractions are 0.83, 0.74 and 0.68 by area. The period of the elliptic points is denoted by n.

periods with integer values. This argument can be tested by controlling the periods of the islands with the fill level.

Figure 6 shows experimental images and numerical results in the form of Poincaré sections for systems with even f_E at various heights greater than half-full. Lobes form in each experiment and the symmetry matches that of the regular islands in the Poincaré sections. The number of lobes is equal to the number of regular islands, just as in the half-full case. The Poincaré sections show that the regular islands are smaller than the islands in the half-full systems with even f_E. The patterns are very sensitive to the fill fractions; the regular islands disappear by changing the fill level just a few per cent. Another difference with the half-full case is that the lobes in the half-full systems stretch mostly in the radial direction. The lobes in these systems are skewed toward the direction of rotation, but the pattern is still rotationally symmetric. As the fill fraction is increased, the lobes are more skewed. When lobes leave the flowing layer they are parallel to the free surface resulting in the slanting.

In the previous section, experimental images show that lobes do not form in half-full tumblers with odd f_E owing to the lack of reinforcement. However, the periods of the islands can be fine tuned to make reinforcement possible by changing the fill fraction. Figure 7 shows experimental and numerical results corresponding to such cases. The Poincaré sections indicate that the periods of the elliptic points are integer values, suggesting that resonance is present.

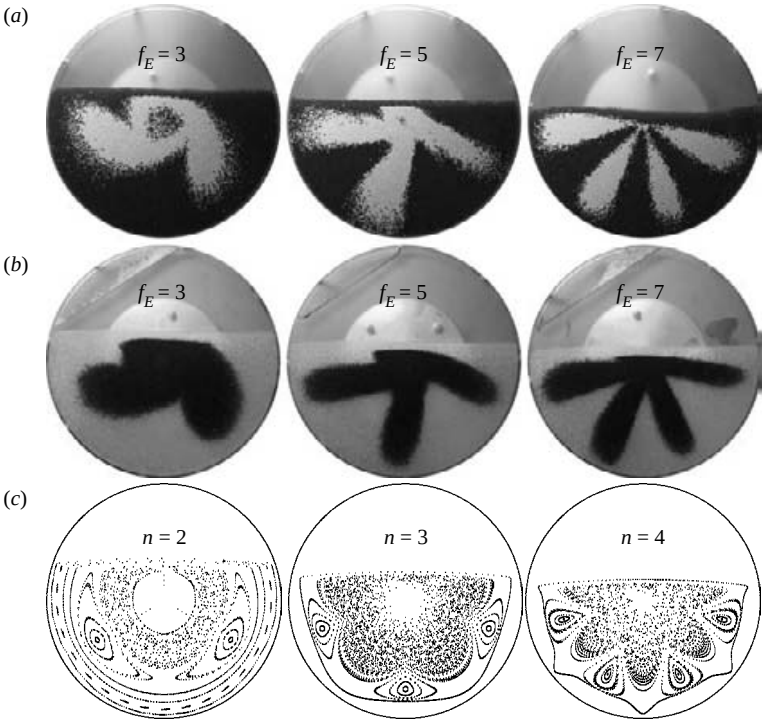

FIGURE 7. Results for a tumbler more than half-full with odd f_E. (*a*) Experimental images from a DGS. The fill fractions are 0.68, 0.62 and 0.57 by area. (*b*) Experimental images from a LGS. The fill fractions are 0.67, 0.61 and 0.58 by area. (*c*) Poincaré sections from numerical simulation. The fill fractions are 0.71, 0.64 and 0.60 by area. The period of the elliptic points is denoted with n.

8. Further analysis of the half-full tumbler

The experiments and Poincaré sections of systems run with even f_E (figure 3) suggest that the model, simple as it is, clearly captures the segregation patterns observed in the system. The experiments and Poincaré sections of systems run with odd f_E (figure 4), on the other hand, do not agree as well when the system is half-full. There is evidence of small lobes at the periphery of the segregated regions in some of the experiments, but the patterns do not match up. The images from the experiments in figures 3 and 4 are only a snapshot of the segregation pattern at a certain instant in time and the pattern that is captured in the image may not necessarily show the general long-time behaviour captured by the Poincaré sections. To gain more understanding of the long-time behaviour of the system, many images of LGS experiments are averaged to form one image representing the segregation pattern of the system. Averaged images for each f_E studied are shown in figure 8. Systems run with even f_E show patterns similar to those of figure 3 – large lobes with the same pattern as the Poincaré sections. Systems run with odd f_E also show clear evidence of smaller islands similar to those in the Poincaré sections of figure 4.

A second issue is the correspondence of lobes and the islands in the Poincaré sections. In experiments, both segregation and collisional diffusion take place, but the model includes neither. Yet experiments clearly show evidence of lobes where islands exist in the Poincaré sections. To what extent do the particles in the lobes remain trapped, as those in the numerically computed Poincaré sections? To investigate

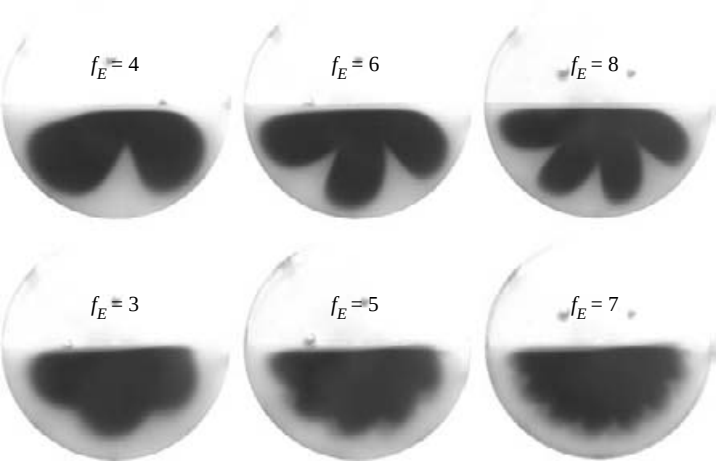

FIGURE 8. Images of LGS experiments capturing the long-time behaviour for all the studied f_E. Each image is made by merging 9000 experimental images. The symmetric placement of regular regions is seen for both the even and odd f_E.

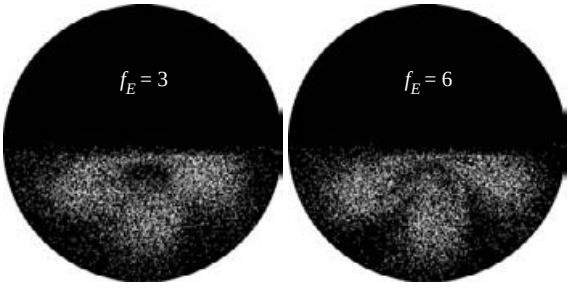

FIGURE 9. Experimental Poincaré sections for systems run with f_E of 3 and 6 cycles rev^{-1}. The images are made using data from particle tracking experiments. Both images show evidence of three lobes.

this issue, a single tracer particle is tracked in a bidisperse LGS for f_E of 3 and 6 cycles rev^{-1}. The Poincaré sections predict three regular islands for each f_E. Figure 9 shows the experimental Poincaré sections corresponding to the two f_E made with the particle tracking data. Both systems show clear evidence of three lobes as predicted by numerically computed Poincaré sections; but in each case, the tracer particle does not remain in a single lobe, rather it fills in the regions of all the lobes owing to collisional diffusion.

The probability distributions of the tracer particle's position show that, statistically, the tracer particle prefers to be at a certain radial position and in one of the three lobes (figure 10). The most probable radial position is between $0.55R$ and $0.6R$ for both f_E. There are three clear peaks in the probability distributions of the tracer particle's angular position in both cases, one corresponding to each of the lobes. The peaks for $f_E = 6$ are more defined, as should be expected since the lobes are more defined in the experiments. Figure 11 shows plots of the angular position of the tracer particle against the angular position the previous revolution. Points near the $y = x$ line are a result of the tracer particle remaining in the same lobe after one revolution. Points away from the $y = x$ line are a result of the tracer particle moving to another

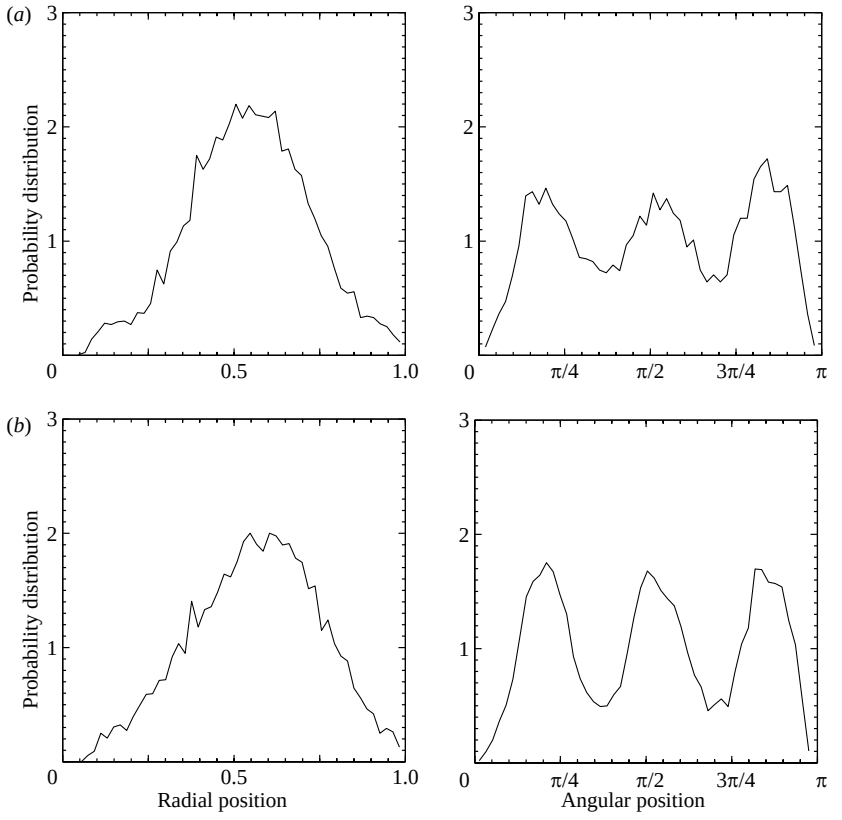

FIGURE 10. Probability distributions of the radial and angular positions for the tracked particle in figure 9. (*a*) $f_E = 3$, (*b*) $f_E = 6$.

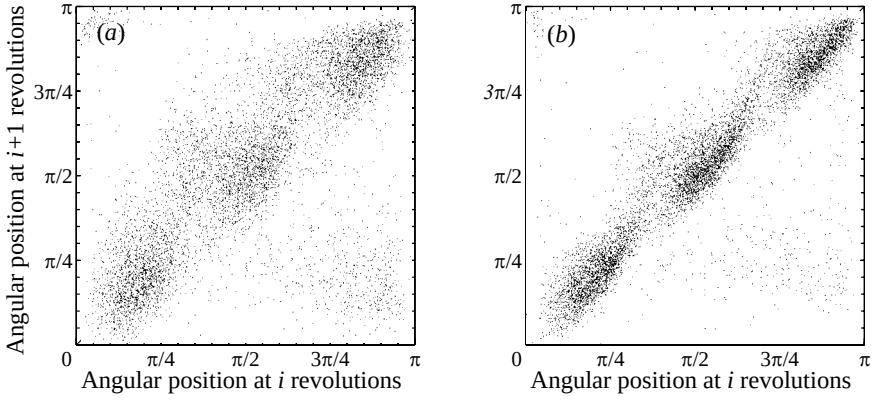

FIGURE 11. Plots of the angular position after $i + 1$ revolutions against the angular position after i revolutions. Points near the $y = x$ line signify that the particle's angular position did not vary much – indicating the particle remained in the same island. (*a*) $f_E = 3$, (*b*) $f_E = 6$.

lobe after one revolution. Both plots in figure 11 show three regions with a higher density of points near the $y = x$ line. These three regions correspond to the three lobes in the experiments. The higher scatter in the plot for the experiment with $f_E = 3$ indicates that the particle is more likely to jump to another lobe after one revolution.

The distribution of times the tracer particle spends in an island is exponential. On average, the tracer particle remains in the same lobe for 5.9 revolutions when $f_E = 6$ and 2.1 revolutions when $f_E = 3$.

9. Conclusions

Size segregation of DGS and LGS in time-periodically forced quasi-two-dimensional tumblers reveals strong similarities. Both systems exhibit similar multi-lobe patterns when subjected to the same forcing, and a relatively simple model describes the patterns. The results are dominated by symmetry considerations and this opens the possibility of tailoring segregated structures by manipulating the forcing. We believe also that to the extent that surface flow in three-dimensional systems is instantaneously one-dimensional (Gilchrist & Ottino 2003), the picture described here may be generalized to three-dimensional systems as well. A challenge, however, is to merge the combined contributions arising from the symmetries of the container (e.g. square or triangular) and the symmetry of the forcing.

Let us close by addressing the issue of the agreement between the experimental results for DGS and LGS. A possible way to compare the systems is in terms of the Bagnold number (Ba), a classical view within the granular literature (Hunt *et al.* 2002). The Bagnold number is defined as $Ba = \rho_p \dot{\gamma} d\epsilon/\mu$ where ρ_p is the particle density, $\dot{\gamma}$ is the shear rate, d is the particle diameter, ϵ is the surface roughness, and μ is the fluid viscosity (Coussot & Ancey 1999). For the systems considered here, Ba ranges from $O(10)$ to $O(10^2)$ for DGS and from $O(10^{-3})$ to $O(1)$ for LGS. These numbers suggest that different mechanisms are at work and that no agreement should be expected. However, considering the systems and the literature on suspensions provides a better view. The states of a suspension are characterized by the value of the Stokes number (St), which is essentially the Reynolds number (Re) based on the particle size and density ($St = \rho_p \dot{\gamma} d^2/\mu$). At low particle inertia (or low St numbers), viscous forces dominate, and stresses scale linearly with $\dot{\gamma}$. This is the so-called 'quenched state', predicted by Koch and co-workers (Koch 1990; Tsao & Koch 1995). No agreement is expected between DGS and LGS. At high St, the stresses scale inertially and are proportional to $\dot{\gamma}^2$. This is the so-called 'ignited state'. A significant result is that the transition from the 'quenched' to 'ignited state' occurs at a St of roughly 10 over a wide range of volume fractions (John Brady, personal communication). In this case the behaviour of DGS and LGS is expected to be nearly identical. The values of St in our experiments range from $O(10^2)$ to $O(10^3)$ for DGS and from $O(1)$ to $O(10)$ for LGS. Our results suggest that agreement may occur at even lower values of St.

One of the main points that emerge from this study is that under various conditions DGS and LGS produce similar segregation patterns, have similar flow properties, and display qualitatively similar dynamic behaviours. This is significant from a research standpoint since LGS offer several experimental advantages over DGS, and therefore result in more controllable experiments which are easier to interpret. Controlling body forces via buoyancy is one example. Perhaps more important is that humidity, electrostatic charging of particles and abrasion, problems that plague even the simplest experiments with DGS, play little or no role in LGS. The absence of the buildup of electrostatic charges or cohesive forces due to moisture in LGS systems makes experiments with small particles possible. It becomes practical to study smaller desktop systems with magnetic fields and therefore altering body forces becomes practical as well. This is difficult to achieve in DGS. Also, with suitable fluids and proper illumination, we can visualize the interior of a granular bed without recourse

to expensive magnetic resonance imaging (MRI) or X-ray instrumentation (Jain *et al.* 2001).

This research was supported by DOE, Office of Basic Energy Sciences.

REFERENCES

Coussot, P. & Ancey, C. 1999 Rheophysical classification of concentrated suspensions and granular pastes. *Phys. Rev.* E **59**, 4445–4457.

Duong, N. H. P., Hosoi, A. E. & Shinbrot, T. 2004 Periodic knolls and valleys: coexistence of solid and liquid states in granular suspensions. *Phys. Rev. Lett.* **92**, 224502.

Gilchrist, J. F. & Ottino, J. M. 2003 Competition between chaos and order: mixing and segregation in a spherical tumbler. *Phys. Rev.* E **68**, 061303.

Hill, K. M., Khakhar, D. V., Gilchrist, J. F., McCarthy, J. J. & Ottino, J. M. 1999 Segregation-driven organization in chaotic granular flows. *Proc. Natl. Acad. Sci. USA* **96**, 11701–11706.

Hill, K. M., Gioia, G. & Amaravadi, D. 2004 Radial segregation patterns in rotating granular mixtures: waviness selection. *Phys. Rev. Lett.* **93**, 224301.

Hunt, M. L., Zenit, R., Campbell, C. S. & Brennen, C. E. 2002 Revisiting the 1954 suspension experiments of R. A. Bagnold. *J. Fluid Mech.* **452**, 1–24.

Jain, N., Khakhar, D. V., Lueptow, R. M. & Ottino, J. M. 2001 Self-organization in slurries. *Phys. Rev. Lett.* **86**, 3771–3774.

Jain, N., Ottino, J. M. & Lueptow, R. M. 2002 An experimental study of the flowing granular layer in a rotating tumbler. *Phys. Fluids* **14**, 572–582.

Jain, N., Ottino, J. M. & Lueptow, R. M. 2004 Effect of interstitial fluid on a granular flowing layers. *J. Fluid Mech.* **508**, 23–44.

Jin, B. & Acrivos, A. 2004 Theory of particle segregation in rimming flows of suspensions containing neutrally buoyant particles. *Phys. Fluids* **16**, 641–651.

Khakhar, D. V., McCarthy, J. J., Shinbrot, T. & Ottino, J. M. 1997 Transverse flow and mixing of granular materials in a rotating cylinder. *Phys. Fluids* **9**, 31–43.

Khakhar, D. V., McCarthy, J. J., Gilchrist, J. F. & Ottino, J. M. 1999 Chaotic mixing of granular materials in two-dimensional tumbling mixers. *Chaos* **9**, 195–204.

Khakhar, D. V., Orpe, V. O. & Ottino, J. M. 2001 Surface granular flows: two related examples. *Adv. Complex Sys.* **4**, 407–417.

Koch, D. L. 1990 Kinetic theory for a monodisperse gas-solid suspension. *Phys. Fluids* A **10**, 1711–1723.

Komatsu, T. S., Inagaki, N., Nakagawa, N. & Nasuno, S. 2001 Creep motion in a granular pile exhibiting steady surface flow. *Phys. Rev. Lett.* **86**, 757–760.

Makse, H. A. 1999 Continuous avalanche segregation of granular mixtures in thin rotating tumblers. *Phys. Rev. Lett.* **83**, 3186–3189.

Ottino, J. M. 1989 *The Kinematics of Mixing: Stretching, Chaos, and Transport*. Cambridge University Press.

Taberlet, N., Richard, P., Valance, A., Losert, W., Pasini, J. M., Jenkins, J. T. & Delannay, R. 2003 Superstable granular heap in a thin channel. *Phys. Rev. Lett.* **91**, 264301.

Thomas, P. J., Riddell, G. D., Kooner, S. & King, G. P. 2001 Fine structure of granular banding in two-phase rimming flow. *Phys. Fluids* **13**, 2720–2723.

Tirumkudulu, M., Tripathi, A. & Acrivos, A. 1999 Particle segregation in monodisperse sheared suspensions. *Phys. Fluids* **11**, 507–509.

Tsao, H.-K. & Koch, D. L. 1995 Simple shear flows of dilute gas-solid suspensions. *J. Fluid Mech.* **296**, 211–245.